Desalination and Water Treatment
www.deswater.com

doi: 10.5004/dwt.2020.25699

190 (2020) 52–61
June

Modeling of surface fouling on the surface of a rotating disk membrane using CFD and numerical study

Soufyane Ladeg[a,*], Nadji Moulai-Mostefa[b], Aissa Ould-Dris[c], Luhui Ding[c]

[a]*Faculty of Science and Technology, University of Tissemsilt, Rue de Bougara, Ben Hamouda, 38004 Tissemsilt, Algeria, Tel./Fax: +213 25 784 608; email: ladeg.soufiane@yahoo.fr (S. Ladeg)*
[b]*Materials and Environmental Laboratory, University of Medea, Ain D'Heb, 26001 Medea, Algeria, email: moulai.nadji@univ-medea.dz (N. Moulai-Mostefa)*
[c]*EA 4297 TIMR, Technological University of Compiegne, 60205 Compiegne Cedex, France, emails: aissa.ould-dris@utc.fr (Ould-Dris), luhui.ding@utc.fr (L. Ding)*

Received 2 July 2019; Accepted 15 February 2020

ABSTRACT

This paper deals with an investigation of the evolution of the thickness of the cake deposited on the surface of a rotating membrane. Therefore, a flowchart was employed to estimate the thickness using CFD results obtained in the microfiltration of a suspension of carbonate of calcium. A usual mathematical model that predicts the filtrate flow was employed. The only unidentified parameter was the internal coefficient of friction (CF) of the cake. The pressure showed a parabolic profile with the radius and the results of the shear stress were found low for a radius of less than 0.04 m. A value of CF was found between 0.05 and 0.1 for all the tests and the two used disks.

Keywords: Microfiltration; Rotating membrane; Fouling; Modeling; CFD

1. Introduction

Fouling on membrane surfaces has been a critical issue and a challenge to researchers and the filtration industry during the last decades. Enhancing the performance of this process by identifying and quantifying the cake thickness or pore blocking is of primary importance [1,2].

The concentration polarization and/or the pore blocking of the membrane are caused by the deposition of suspended colloids and particles on the surface, which lead to a membrane fouling [3,4]. In addition, a high solute concentration is created near the membrane area which can generate an osmotic pressure by which the solute can return to the solvent phase in the case of low pressure applied to the liquid [5].

To avoid this phenomenon and cake resulting in the membrane surface, cross-flow can be used; this technique has widely been employed to concentrate solutes from solutions [1,3]. In cross-flow filtration, the bulk flow occurs along the filtering membrane and perpendicular to the filtrate flow. Accordingly, high fluid velocities are necessary to decrease the buildup of concentrate species on the membrane surface [1].

Several models were proposed in the literature to estimate the cake thickness and flux in cross-flow filtration. Song [6] investigated the flux drop in ultrafiltration and microfiltration and developed a mechanistic model to predict the time-dependent flux and the time needed to reach the steady-state. Paipuri et al. [7] proposed a model that can predict the concentration polarization and the particle deposition in cross-flow membrane filtration. They employed Navier–Stokes and convection–diffusion equations to solve the cross-flow hydrodynamics and filtrate distribution. The results were validated after being compared to many predictions

* Corresponding author.

that were suggested by other computational models and to empirical results found in the literature. In the aim of providing one differential equation for the cake thickness as a function of time, Foley et al. [8] developed a theoretical model of cross-flow filtration that considers the particle polydispersity; their model associates classical theory of filtration with the rule of the cut-off particle diameter using analysis of the hydrodynamic forces. Their work brought in interesting results; the model can successfully predict both the observed behavior of the flux and cake thickness as well as the behavior of the medium-specific resistance of the cake. Chen and Hsiau [9] developed an experimental model to expect the cake thickness on the filter surface. It was found that the cake filter was influenced by the cake thickness and the superficial velocity of filtration; it was also deduced that the solidosity and specific resistance of the cake increased with the superficial velocity. Benkahla et al. [10] studied the fouling process in cross-flow filtration of $CaCO_3$ suspension. They increased and decreased the transmembrane pressure (TMP) in steps at steady velocity to form cycles; they deduced that the cake thickness growth was restricted by the shear stress acting on its surface. Broeckmann et al. [11] introduced two models to explain the acting of particles where they considered the adhesive forces between the particles and membrane surface, which, in fact, dramatically influence the cake formation and the efficiency of backflushing. The second model evaluates the impact of particles and membrane pore size dispersal on both cake layer deposition and pore-clogging and, their mutual dependencies. It was noticed that the data they simulated reach agreement with the experimental results. On the other side, Ould-Dris et al. [12] investigated the consequence of repeated variations of TMP, concentration, and velocity on the particle cake of a mineral solute of carbonate of calcium ($CaCO_3$) formed on an organic membrane during the microfiltration. They found that during the cake formation, the filtrate flux was controlled by the normal shear stress on the cake area. Hwang et al. [13] studied the non-uniformity of the cake formation and filtrate flux in rotating-disk dynamic microfiltration of fine particles. They used CFD to simulate the distribution of velocity and shear stress on the membrane surface, and they proposed a model that can estimate the cake formation based on a force balance model. The results demonstrated that the local filtration flux increases in parallel with the critical particle size.

This paper aimed at establishing a review of existing models for the determination of filtrate flux in dynamic cross-flow filtration and then presenting a new model based on the quantification of cake layer thickness on the surface of a rotating disk membrane. In other words, the stability of the cake layer top was studied. Hence, we determined the adequate friction factor of the top deposit of the cake that sets the cake thickness by computing the corresponding shear stress and pressure using CFD results. Consequently, we set conditions between the normal shear stress, friction factor, and tangential shear stress that can build the cake thickness, while the monolayer cake thickness was supposed to be equivalent to the average cake particle diameter. In addition, the flux values that have been determined in previous works [14,15] were used for the validation and comparison of the proposed model using the same conditions of flow rate, viscosity, and rotating velocity.

2. Theory

Fig. 1 shows the feed suspension flow where is focused normal or tangential to the membrane. This type of flow pattern is called tangential flow and is most often employed in large volume laboratory and process applications targeting solute concentration [13].

The permeate flux can be described by the Darcy law for the cake and membrane resistances in series:

$$J_f = \frac{\Delta P}{\mu\left(R_m + R_c\right)} \tag{1}$$

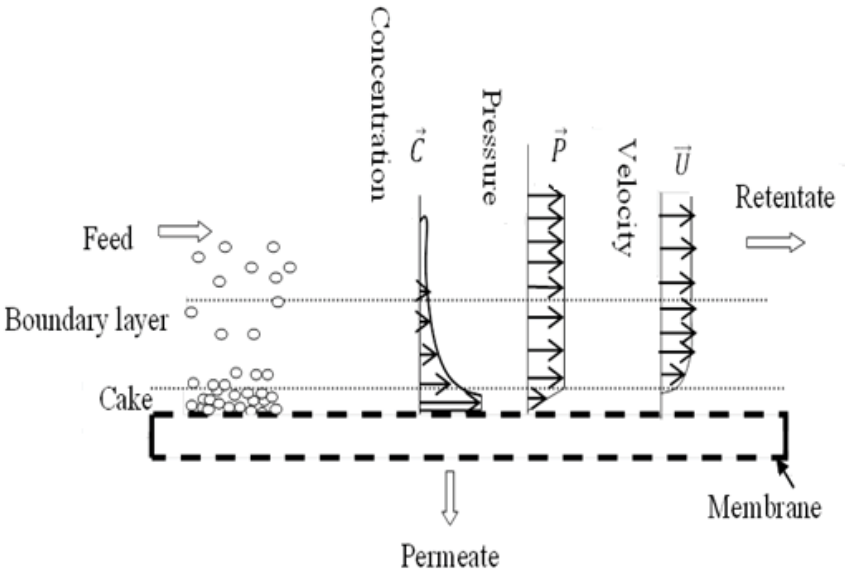

Fig. 1. Evolution of various parameters at the membrane-solution interface.

where ΔP is the TMP, μ is the filtrate viscosity (Pa s), R_m is the intrinsic membrane resistance (m^{-1}), and R_c is the cake resistance (m^{-1}).

The amounts of μ and R_m remain constant during filtration. The flux declines when the value of R_c increases because of the cake deposition on the membrane area. For that, we consider the cake layer of $CaCO_3$ as an incompressible porous media with a homogeneous structure. Consequently, the cake resistance can be defined by the Carman–Kozeny equation as:

$$R_{\text{cake}} = 180\frac{\left(1-\varepsilon_c\right)^2}{\left(d_p\right)^2\varepsilon_c^3}\delta \tag{2}$$

where ε_c is the porosity of the cake, d_p is the average particle diameter (m), and δ is the cake thickness (m).

If Eq. (1) and (2) are used to provide the permeate flux, the cake thickness which deposits on the membrane area must be known. The cake will grow over time until the flux is steady-state. In the following subsection, a model is presented to expect the steady-state cake thickness on the membrane by defining the filtrate flux and the cake resistance where the shear stress and pressure are determined by a digital simulation under the experienced conditions. The model is based on the condition that the thickness of the cake deposit can grow on the membrane surface until the normal stress cannot maintain additional particle monolayer under the shear stress applied by the liquid.

The top particle deposited on the membrane will be subject to shear stress generated by the liquid at its surface:

$$\tau = \mu_s\frac{\partial V_\theta}{\partial z} \tag{3}$$

where τ is the shear stress (Pa) that can erode the top layer of the cake [12].

The critical balance of forces applied to the upper monoparticle layer to be eroded is given by Eq. (4).

$$\tau = \mu_f N \tag{4}$$

where μ_f is the coefficient of friction and N is the normal shear stress (Pa).

In this case, the normal shear stress can be written as the pressure drop over the top particle monolayer [12]:

$$N = \Delta P_N = \left|\frac{\partial p}{\partial z}\right|_{z=\delta}\bar{d}_p \tag{5}$$

From Eq. (1) and using the Kozeny–Carmen equation, we can express the local filtrate flux with the local resistance of the cake. As is constant and by combining the Kozeny–Carmen equation and Eq. (1), we can express the normal stress on the monoparticle top layer:

$$N = \left|\frac{\partial p}{\partial z}\right|_{z=\delta}d_p = J\mu 180\frac{\left(1-\varepsilon_c\right)^2}{\left(\varphi d_p\right)^2\varepsilon_c^3}d_p \tag{6}$$

Furthermore, Eq. (4) can be rewritten as:

$$\tau = 180\mu_f J\mu\frac{\left(1-\varepsilon_c\right)^2}{\left(\varphi d_p\right)^2\varepsilon_c^3}d_p \tag{7}$$

This set of equations can let to determine the local thickness and permeate flux that can allow calculating the average filtrate flux ($\bar{J}$).

$$\bar{J} = \frac{1}{S}\int_0^s J\,ds = \frac{1}{R^2}\int_0^s J2rdr \cong \frac{\left(\sum_i^n 2J_i r_i\Delta r\right)}{R^2} \tag{8}$$

The average flux calculated by Eq. (8) must be found equal to the experimental flux by adjusting the friction coefficient. Benkahla et al. [10] found that the values of μ_f ranged from 0.15 to 0.25.

The variations of the dynamic pressure on the membrane surface can be deduced using Navier–Stokes equations in the laminar flow regime [16]. These equations cannot, unfortunately, give the accurate variation of the pressure for the two used disk geometries. However, Torras et al. [16] and Bouzerar et al. [17] utilized these equations to interpret their experimental results and compared them to Eq. (9).

$$P\left(r\right) = P_0 + 0.5\rho k^2\omega^2 r^2 \tag{9}$$

where P_0 is the pressure (Pa) at the symmetry axis (r = 0), ρ is the density of the liquid (kg m^{-3}), ω is the angular velocity (rad s^{-1}), r is the radial position (m), and k is the velocity factor (its value is equal to 0.42 for the disk without vanes and 0.84 for the disk with vanes).

3. Model flowchart

Taking the equations presented above as a basis, the cake thickness and the filtrate flux were simulated using the flowchart depicted in Fig. 2. The same values of the empirical constants were used in CFD simulation and flowchart calculation steps.

The average permeate fluxes obtained by computation using the flowchart were compared with the mean experimental values obtained by Brou et al. [14] and Bouzerar et al. [15] in the same conditions. The coefficient of friction was adjusted in order to obtain the predicted values of flux close to the experimental ones.

4. Experimental device

Fig. 3 illustrates two geometries of the rotating disk membranes (RDM). They were utilized in the filtration of chicory juice [18], milk effluent [19,20], and $CaCO_3$ suspension [14,15]. The flat membrane was fixed on the cover of the cylindrical housing in front of the disk whether it is equipped with vanes or not. Therefore, the simulations were performed on the same physical model. The software CFD description and the geometry creation by Ansys Fluent Workbench have been discussed in details in our previous work [21]. The membrane was a symmetric nylon one

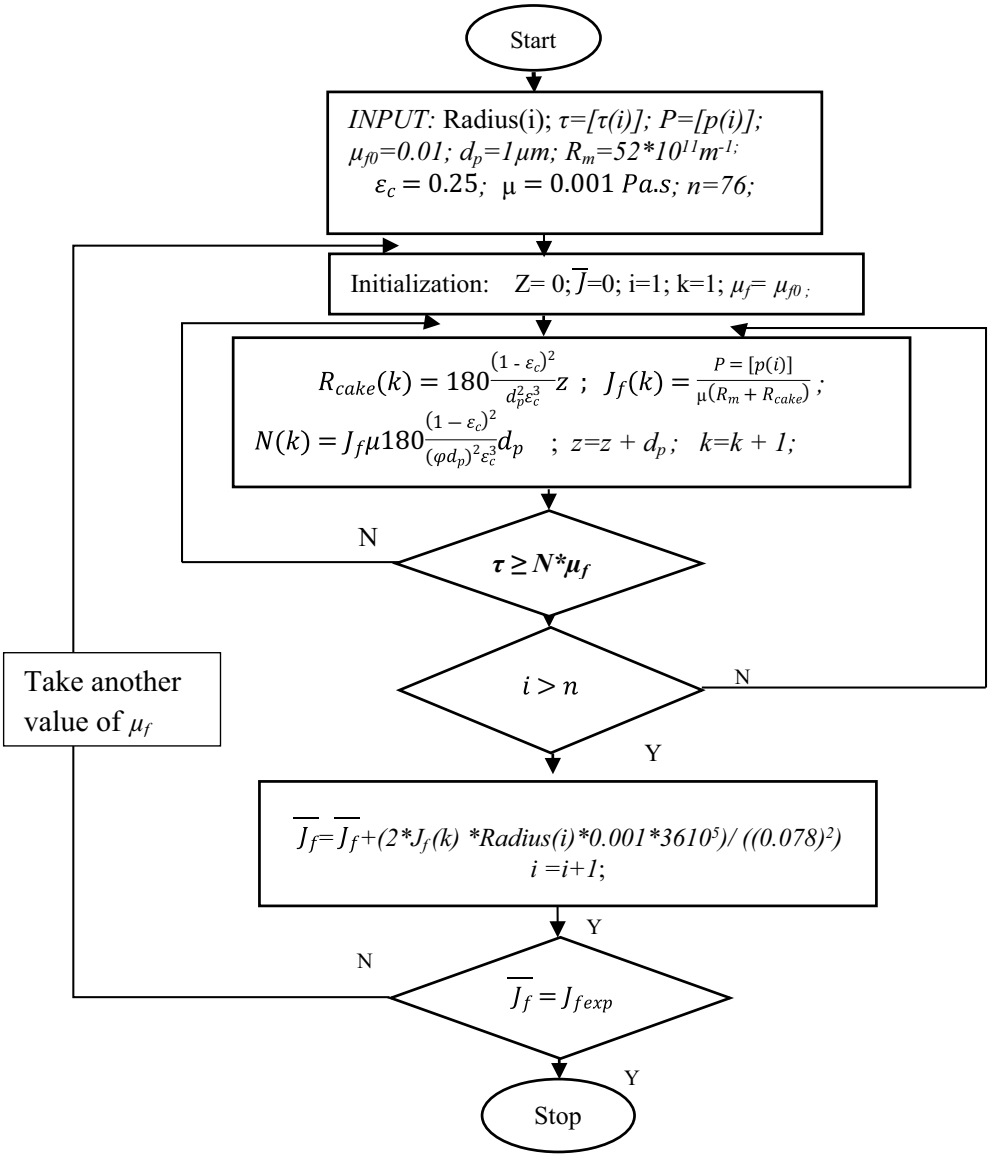

Fig. 2. Model flowchart used in estimating the cake thickness.

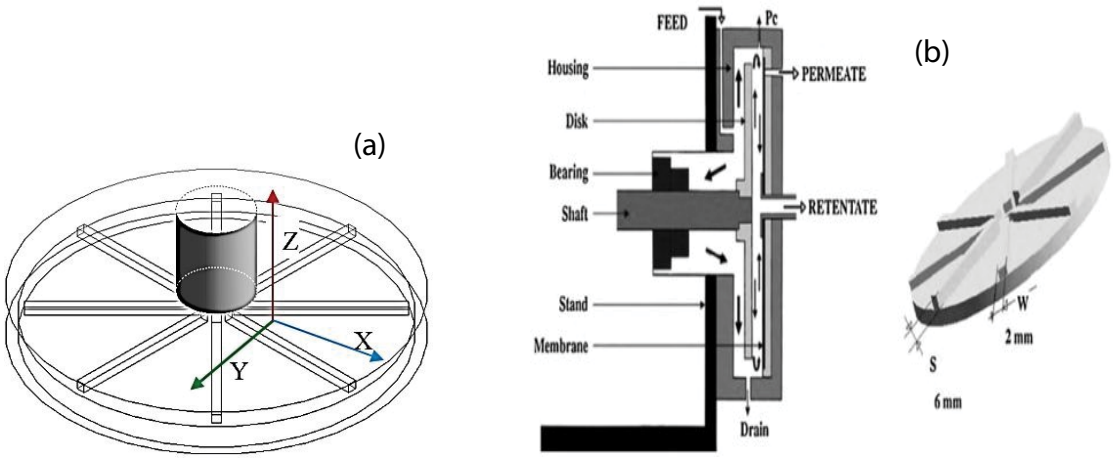

Fig. 3. Schematic representation of the simulating model (a) with the experimental RDM (b).

(Ultipor, PALL. East Hills, USA) with 0.2 m pores and a filtration resistance R_m of 52×11^{11} m^{-1} [17].

5. Results and discussion

Fig. 4 shows the variations of the shear stress vs. the membrane radius and the distribution of the shear stress on the membrane of the disk equipped with vanes. The used values were deduced from the results of the microfiltration of a suspension of $CaCO_3$ [14]. It was observed that the shear stress was very low when the radius is between 0.01 and 0.04 m (Fig. 4a); this can be interpreted by the lower tangential velocity that was then created in the rotating disk and the high viscosity of the suspension of $CaCO_3$. Up to 0.04 m, the shear stress increases with the radius in an irregular manner. The curve takes a wavy form (undulated) for the radius values ranged between 0.04 and 0.07 m. However, for a radius value higher than 0.07 m, the shear stress increases and reaches a maximum value of 310 Pa for a radius around 0.075 m. This behavior is not consistent with the curve obtained for milk effluent [19], especially for radius around a value of 0.04 m. Fig. 4b shows clearly that the distribution of the shear stress on the membrane is not uniform, this result was also confirmed by Hwang et al. [13] using the suspension of polymethyl methacrylate. The major part of the region of the high shear stress is on the rim of the surface (red, yellow, and green color), and the low shear stress value is in the major part of the surface (blue color). The tangential velocity is related to the rotational velocity and membrane radius, this velocity generates an augmentation in shear stress and pressure. These results agree well with those obtained by Torras et al. [16]. It can be deduced that the high tangential velocity has a great effect on the variation of the shear stress on the membrane surface and by consequence in reduction or enhancement of permeate flux, especially for radius values that ranged from 0.01 to 0.05 m. The great density of $CaCO_3$ may make the distribution of the shear stress on the surface non-uniform, which influences the variation of the cake thickness.

Fig. 5a presents the evolution of the shear stress as a function of radius for a disk without vanes and rotation velocity of 2,000 rpm. The shear stress is weak in the area where the radius varies between 0.01 and 0.04 m; the maximum value reaches 8 Pa in this part of the membrane. This can be interpreted by the low tangential velocities in this region. Fig. 5b clearly shows the region (colored in blue) which has low values of shear stress where the distribution is relatively uniform compared to the disk equipped with vanes. As a result, the presence of vanes and the fluid density make the distribution of the stress non-uniform on the membrane. It was also noticed that above the value of 0.04 m of the radius (Fig. 5a), the shear stress increases rapidly until reaching the maximum value of 140 Pa near the radius of 0.07 m.

The values of pressure and shear stress were used to evaluate their effects on the formation of the deposited layer in the case of a smooth disk. The variation of the pressure vs. radius has a parabolic profile (Fig. 6), essentially for radius values ranging between 0.01 and 0.07 m. The pressure increases rapidly with the radius; it is distributed more evenly over the area of the membrane in comparison with the shape of the shear stress. Pressure values calculated by CFD in the case of a disk with vanes are identical to those obtained in the radius region ranging from 0.01 to 0.055 m. Above this radius portion, the pressure values increase and become superior to those obtained with a smooth disk; they reach a value of 3 bar for a value of the radius of 0.07 m. Moreover, the dynamic pressure varies linearly with the density of $CaCO_3$ suspension and the square of the radius and the angular velocity, according to a linear relationship (Eq. 9) that can be deduced from the Navier–Stokes equations [16]. On the other hand, Bouzerar et al. [17] also found in their study that the density and viscosity of $CaCO_3$ increase the TMP from 1.4 to 2.3 bars when they increased the concentration of $CaCO_3$.

Fig. 7 illustrates the deposit thickness variation as a function of radius for a rotation speed of 2,000 rpm (disk with vanes) and for different coefficients of friction (0.03,

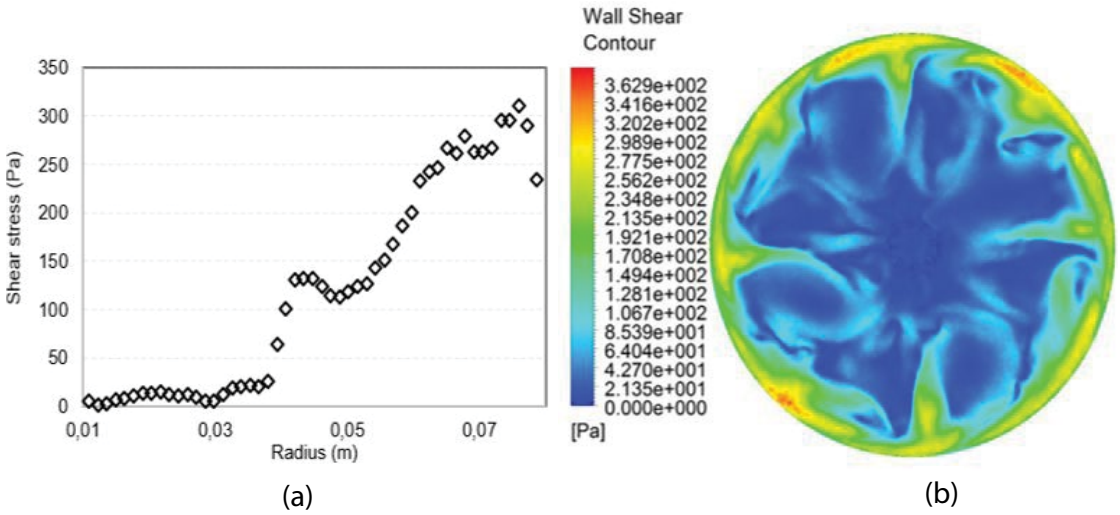

Fig. 4. (a and b) Shear stress variation vs. radius in the case of microfiltration of $CaCO_3$ suspension (Rotating disk with vanes, w = 2,000 rpm, T = 25°C).

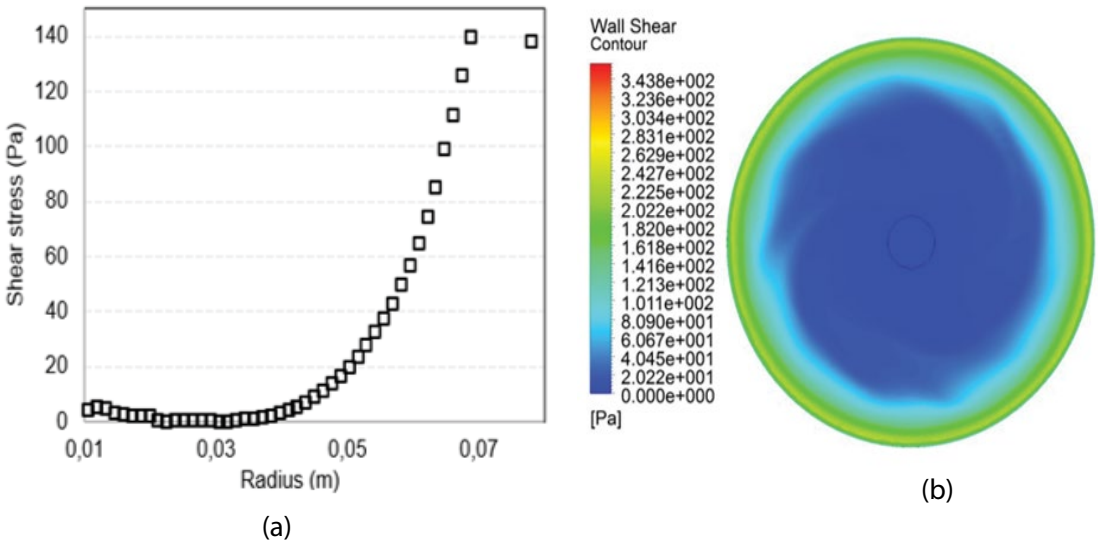

Fig. 5. (a and b) Shear stress variation vs. radius; microfiltration of $CaCO_3$ suspension at 2,000 rpm (Rotating disk without vanes, T = 25°C).

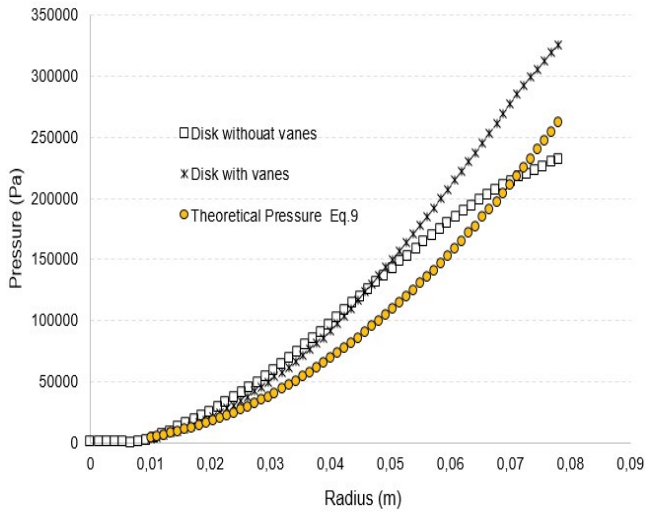

Fig. 6. Pressure variation vs. radius; microfiltration of $CaCO_3$ suspension at 2,000 rpm (T = 25°C).

0.05, 0.1, and 0.3). It can be seen that for the four cases, the variations have the same profiles, but the calculated thicknesses and filtrate fluxes are different and depend on the coefficient of friction (μ_f). The greatest thickness is obtained for a μ_f equal to 0.3 where it reaches a value of 0.003 m and the smallest value of the thickness (0.1×10^{-4} m) was obtained for a value of μ_f of 0.03. For each μ_f, the large variations in thickness are located over a radius variation range (from 0.015 to 0.025 m). This thickness gradually decreases from the value of the radius which is greater than 0.03 m. This corresponds to the results presented in Fig. 4; it was observed that from a radius equal to 0.04 m, the shear stress increases leading to a decrease of the deposited layer. However, the values of μ_f were found by some researchers between 0.1 and 0.3 [22] and by others between 0.01 and 0.05 [23], a maximum value of 0.03 was found by Broeckmann et al. [11]. Moreover, in the region of the membrane where the radius is between 0.04 and 0.08 m, the pressure is also high (Fig. 6), which results in an accumulation of the deposit particles on the membrane surface [24]. In our case, the results depicted in Fig. 7 shows the effect of the shear stress and not of the pressure especially in the area where the radius is greater than 0.04 m. Therefore, it can be concluded that the values of the shear stress have increased the erosion effect of the deposited layer, despite the high values of pressure. The stability of this layer can be controlled by the high values of shear stress.

Fig. 8 shows the fluctuation of the thickness of the deposited layer vs. radius for different μ_f on the membrane surface of a smooth disk. The graphs present the same shapes as those obtained with a disk equipped with vanes where only a single peak was observed at a radius of 0.032 m. Thus, this peak reaches different values depending on μ_f; it is between 0.017 and 0.005 m for a value of μ_f varying between 0.1 and 0.03. Hence, for a thinner deposit layer, a value of μ_f lower than 0.03 is required.

The shear stress and pressure effects are well observed for a disk without vanes. The pressure increases gradually as a function of radius ($0 \le R \le 0.035$ m) and in parallel, the deposited layer also accumulates progressively up to the radius of 0.032 m where it reaches the maximum value. In this part of the membrane, the values of the shear stress are generally low. Above this point of the radius (0.032 m), the shear stress increases with the pressure, but the thickness of the deposited layer decreases progressively along the radius to the peripheral of the membrane. This can be described by the efficiency of the shear stress on the erosion of the deposited layer (up to 0.043 m) in front of the pressure. However, in the region where the radius is less than 0.015 m, there is also a small thickness of the deposited layer, although the values of the shear stress are low in this part of the membrane; this can be explained according to the low pressure which prevents the agglomeration of particles in this region.

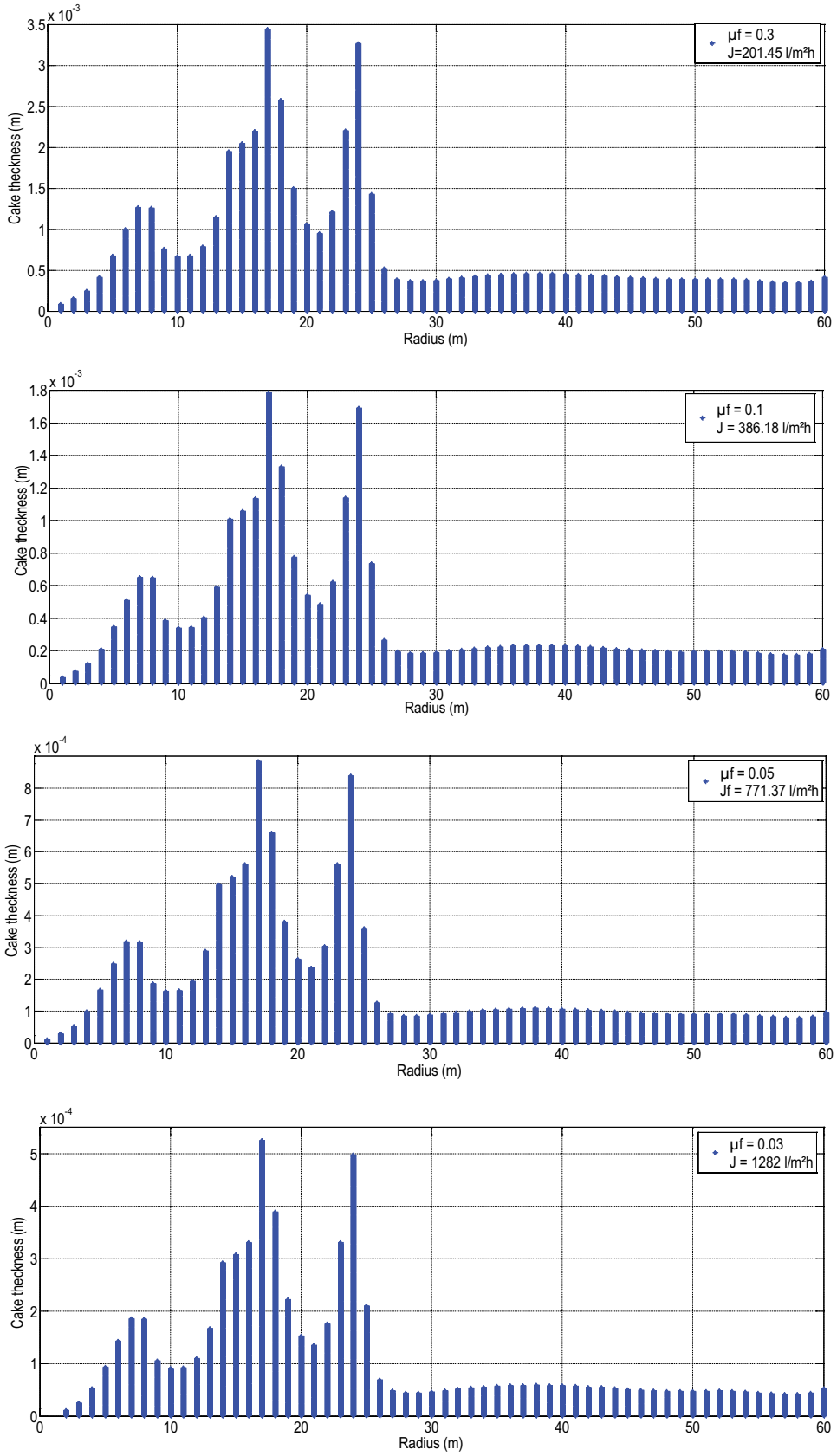

Fig. 7. Thickness variation vs. radius; microfiltration of $CaCO_3$ suspension at 2,000 rpm (Rotating disk equipped with vanes; μ_f = 0.1, 0.3, 0.03, and 0.05; T = 25°C).

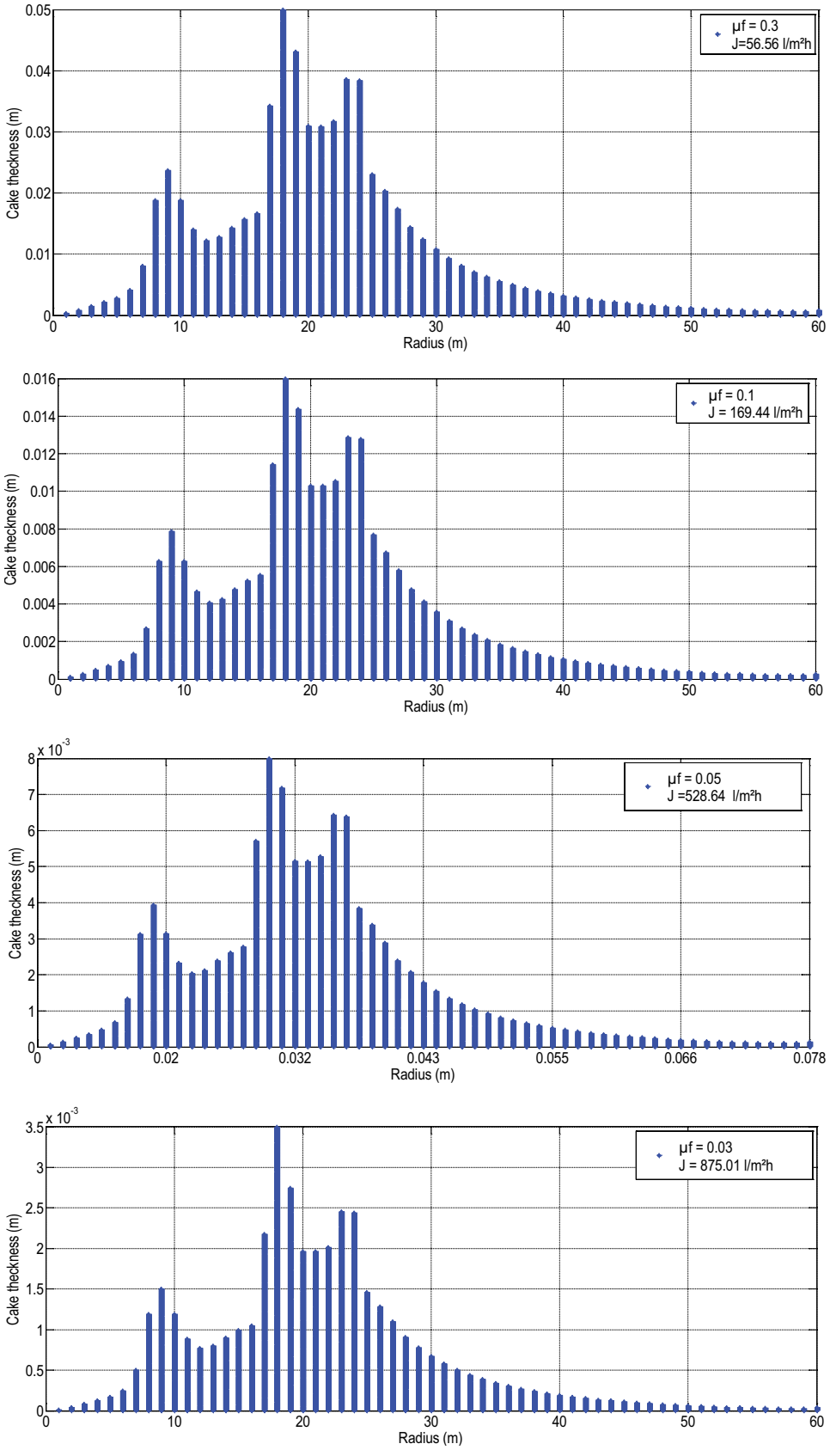

Fig. 8. Thickness variation vs. radius; microfiltration of $CaCO_3$ suspension at 2,000 rpm (Rotating disk without vanes; μ_f = 0.1, 0.3, 0.03, and 0.05; T = 25°C).

Table 1
Maximum and minimum thickness values of the deposited layer for different values of μ_f and for two types of disks (with and without vanes)

	Disk equipped with vanes				Smooth disk			
Coefficient of friction (μ_f)	0.3	0.1	0.05	0.03	0.3	0.1	0.05	0.03
Maximal values of the deposit layer thickness × 10^4 (m)	34	17	8.8	5.25	500	158	79.5	34.8
Minimal values of the deposit layer thickness × 10^4 (m)	0.8	0.34	0.1	0.1	3.8	1.13	0.57	0.1

The role of the vanes can be demonstrated by the comparison between the optimal obtained results of the thickness of the deposited layer (Table 1) for different μ_f and using a disk that might be equipped with vanes or not. Thus, it seems that for a low μ_f (0.03), the maximum and minimum values of the deposited layer thickness are, respectively, 5.25×10^{-4} and 0.1×10^{-4} m (disk with vanes). However, for a disk without vanes (smooth disk), the maximum and minimum thickness values oscillate between 34.8×10^{-4} and 0.1×10^{-4} m. These findings demonstrate the role of vanes in the removal of the deposited layer.

The flux of filtrate was evaluated for each μ_f using the values of pressure and shear stress (calculated by CFD) as a function of radius. The calculated values of flux were compared with those obtained experimentally by some authors [14,15] for disks equipped or not with vanes. The flux found by the theoretical model for a rotation speed of 2,000 rpm and a disk with vanes, varies between 1,282 L/h m² for a value of μ_f equal to 0.03 and 201.45 L/h m² for μ_f equal to 0.3. This means that for the flux to be close to the experimental value, the coefficient of friction must be less than 0.1 and greater than 0.05. To make a comparison between the calculated flux values using the two filtration models, the variation of the flux is represented as a function of μ_f (Fig. 9). The obtained results show a decrease according to a power function of the filtrate flux as a function of μ_f. Bouzerar et al. [15] found a value of flux about 440 L/h m² for a rotation speed of 1,500 rpm. In another study [4], they found a flux value of 1,050 L/h m² for a rotation speed of 2,000 rpm. Moreover, the difference between the flux values is well-observed between the two filtration models. The presence of vanes enhances the flux by contributing to the increase of shear stress and reducing the width of the cake.

From a preliminary study, it was found that the value of the coefficient of friction must be less than 0.1 and greater than 0.05 to obtain the permeate flux compatible with the flux measured experimentally. This result was confirmed for the two membrane filtration modules. The sensitivity of the model used in this investigation is well observed in Fig. 9, where it was noted that μ_f and the filtrate flux are in the same order of magnitude as those found by other authors [14,15,23].

The amassing of the solute on the vicinity of the membrane can be described in two ways, either by the filtration-cake description or by a description according to the theory of the film [25]. In most cases, when the TMP is sufficiently high, a particle cake is formed on the membrane which limits the filtrate flux [13]. Thus, it can be deduced that the high coefficient of friction (μ_f) and high-pressure values are the two main factors favorable for the colloidal particles to accumulate and consequently to produce a deposited layer on the membrane surface.

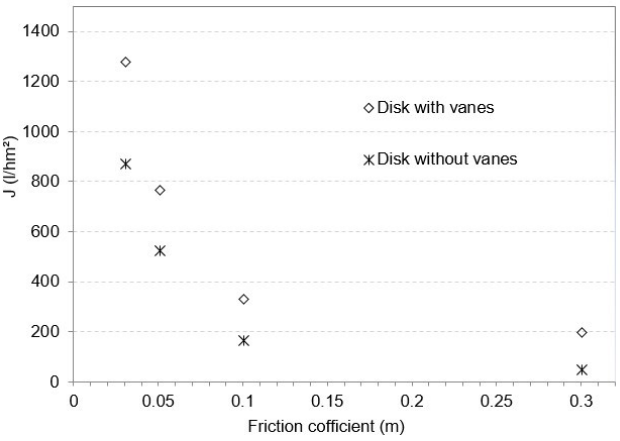

Fig. 9. Flux variation vs. friction coefficient.

6. Conclusion

In this study, an investigation was carried out regarding the distribution of the accumulating layer thickness on the surface of the membrane and the effectiveness of the shear stress in the erosion of the deposited layer. For a disk equipped with vanes, the deposited layer undergoes an erosion effect twice in the radius region between 0.01 and 0.04 m and the maximum thickness is less than that found in the case of a disk without vanes. The coefficient of friction has a significant effect on the formation of the cake layer on the membrane, not to mention the effect of the pressure on this phenomenon. A suitable value for the coefficient of friction has been found which gives a filtrate flux closer to that obtained experimentally.

It must be mentioned that the benefit of this investigation is to show the role of the coefficient of friction in improving the calculation of permeate flux.

Acknowledgment

This research was carried out with the support of the Grant Tassili (13 MDU889) between Algerian and French Governments.

Symbols

d_p — Average particle diameter, m
$\bar{J}$ — Average flux, l h^{-1} m^{-2}

k — Velocity factor
N — Normal shear stress, Pa
P — Transmembrane pressure, Pa
P_0 — Pressure at the symmetry axis, Pa
R_c — Cake resistance, m^{-1}
R_m — Intrinsic membrane resistance, m^{-1}
r — Radial position, m
V_θ — Azimuthal Velocity, m s^{-1}
δ — Cake thickness, m
μ — Filtrate viscosity, Pa s
μ_f — Coefficient of friction
ρ — Density of the liquid, kg m^{-3}
τ — Shear stress, Pa
ϕ — Sphericity of particles
ω — Angular velocity, rad s^{-1}
ε — Porosity of the cake

References

[1] W.M. Lu, K.J. Hwang, S.C. Ju, Studies on the mechanism of cross-flow filtration, Chem. Eng. Sci., 48 (1993) 863–872.
[2] S. Mondal, S. De, A fouling model for steady state crossflow membrane filtration considering sequential intermediate pore blocking and cake formation, Sep. Purif. Technol., 75 (2010) 222–228.
[3] R.W. Field, D. Wu, J.A. Howell, B.B. Gupta, Critical flux concept for microfiltration fouling, J. Membr. Sci., 100 (1995) 259–272.
[4] R. Bouzerar, M.Y. Jaffrin, L. Ding, P. Paullier, Influence of geometry and angular velocity on performance of a rotating disk filter, AIChE J., 46 (2000b) 257–265.
[5] G.B. Van Den Berg, C.A. Smolders, Flux decline in ultrafiltration processes, Desalination, 77 (1990) 101–133.
[6] L. Song, Flux decline in crossflow microfiltration and ultrafiltration: mechanisms and modeling of membrane fouling, J. Membr. Sci., 139 (1998) 183–200.
[7] M. Paipuri, S.H. Kim, O. Hassan, N. Hilal, K. Morgan, Numerical modeling of concentration polarization and cake formation in membrane filtration processes, Desalination, 365 (2015) 151–159.
[8] G. Foley, D.M. Malone, F. Mac Loughlin, Modelling the effects of particle polydispersity in crossflow filtration, J. Membr. Sci., 99 (1995) 77–88.
[9] Y.S. Chen, S.S. Hsiau, Cake formation and growth in cake filtration, Powder Technol., 192 (2009) 217–224.
[10] Y.K. Benkahla, A. Ould-Dris, M.Y. Jaffrin, D. Si-Hassen, Cake growth mechanism in cross-flow microfiltration of mineral suspensions, J. Membr. Sci., 98 (1995) 107–117.
[11] A. Broeckmann, J. Busch, T. Wintgens, W. Marquardt, Modeling of pore blocking and cake layer formation in membrane filtration for wastewater treatment, Desalination, 189 (2006) 97–109.
[12] A. Ould-Dris, M.Y. Jaffrin, D. Si-Hassen, Y. Neggaz, Analysis of cake build-up and removal in cross-flow microfiltration of $CaCO_3$ suspensions under varying conditions, J. Membr. Sci., 175 (2000) 267–283.
[13] K.J. Hwang, S.E. Wu, Y.L. Hsueh, Analysis on the nonuniformity of cake formation in rotating-disk dynamic microfiltration, Sep. Purif. Technol., 198 (2018) 16–24.
[14] A. Brou, L. Ding, P. Boulnois, M.Y. Jaffrin, Dynamic microfiltration of yeast suspensions using rotating disks equipped with vanes, J. Membr. Sci., 197 (2002) 269–282.
[15] R. Bouzerar, L. Ding, M.Y. Jaffrin, Local permeate flux–shear–pressure relationships in a rotating disk microfiltration module: implications for global performance, J. Membr. Sci., 170 (2000a) 127–141.
[16] C. Torras, J. Pallares, R. Garcia-Valls, M.Y. Jaffrin, Numerical simulation of the flow in a rotating disk filtration module, Desalination, 235 (2009) 122–138.
[17] R. Bouzerar, P. Paullier, M.Y. Jaffrin, Concentration of mineral suspensions and industrial effluents using a rotating disk dynamic filtration module, Desalination, 158 (2003) 79–85.
[18] Z. Zhu, S. Ladeg, L. Ding, O. Bals, N. Moulai-Mostefa, M.Y. Jaffrin, E. Vorobiev, Study of rotating disk assisted dead-end filtration of chicory juice and its performance optimization, Ind. Crops Prod., 53 (2014) 154–162.
[19] L. Ding, O. Al-Akoum, A. Abraham, M.Y. Jaffrin, Milk protein concentration by ultrafiltration with rotating disk modules, Desalination, 144 (2002) 307–311.
[20] J. Luo, L. Ding, Y. Wan, P. Paullier, M.Y. Jaffrin, Fouling behavior of dairy wastewater treatment by nanofiltration under shear-enhanced extreme hydraulic conditions, Sep. Purif. Technol., 88 (2012) 79–86.
[21] S. Ladeg, Z. Zhu, N. Moulai-Mostefa, L. Ding, M.Y. Jaffrin, CFD simulation of the distribution of pressure and shear rate on the surface of rotating membrane equipped with vanes for the ultrafiltration of dairy effluent, Arabian J. Sci. Eng., 43 (2018) 2237–2245.
[22] K.J. Jeon, Y.W. Jung, A simulation study on the compression behavior of dust cakes, Powder Technol., 141 (2004) 1–11.
[22] F. Radjai, L. Brendel, S. Roux, Nonsmoothness, indeterminacy, and friction in two-dimensional arrays of rigid particles, Phys. Rev. E, 54 (1996) 861–873.
[23] Y. Lee, M.M. Clark, Modeling of flux decline during crossflow ultrafiltration of colloidal suspensions, J. Membr. Sci., 149 (1998) 181–202.
[24] W.R. Bowen, F. Jenner, Theoretical descriptions of membrane filtration of colloids and fine particles: an assessment and review, Adv. Colloid Interface Sci., 56 (1995) 141–200.